Journal of Materials Science: Materials in Electronics (2019) 30:19854–19861
https://doi.org/10.1007/s10854-019-02352-3

The role of interface traps, series resistance and (Ni-doped PVA) interlayer effects on electrical characteristics in Al/p-Si (MS) structures

Selçuk Demirezen[1]

Received: 12 June 2019 / Accepted: 10 October 2019 / Published online: 15 October 2019

Abstract
The main point of this article is to examine in detail the effects of interface/surface states (Nss), series resistance (Rs) and (Ni-doped PVA) polymer interlayer on current–voltage (I–V) and frequency dependent capacitance–voltage (C–V) properties at room temperature. Some main diode parameters such as reverse-saturation current (I_s), ideality factor (n), barrier height (BH) ($=\Phi_B$(I–V)), R_s, and rectification ratio ($RR=I_F/I_R$) at ± 3 V were calculated from the linear part of LnI–V plot as 2.14×10^{-9} A, 1.606, 0.750 eV, 30.5 Ω, and 10^6, respectively. Energy dependent values of N_{ss} were also extracted from the I–V data by considering voltage dependent BH and *n* they decrease from mid-gap of Si towards the bottom of valance band (E_v) almost as exponentially. The doping atoms (N_a), Fermi energy level (E_F), (Φ_B(C–V)), and depletion layer width (W_D) were also calculated from the reverse bias C^{-2}–V curves as function of frequency. The achievement of obtained results that manufactured (Ni-PVA) interlayer provide better performance in respect of lower values of leakage current, N_{ss}, R_s, and higher values of RR and shunt resistance. The dielectric value of (Ni-PVA) interlayer was found as 1.44 from the interlayer capacitance ($C_i=\varepsilon'\varepsilon_o A/d_i$) even at 20 kHz and this is higher than the dielectric value of SiO_2 at 20 kHz. However, this value can be increased by increasing a dopant level of Ni until 5–7%. Therefore, this interlayer can be successfully use an alternative interface layer compared to traditional oxide interlayers.

1 Introduction

In last decades, researchers are focused on the metal/semiconductor (MS) type Schottky barrier diodes (SBDs) or structures with an interlayer such as oxide and organic/polymer by considering their importance in electronic and optoelectronic devices [1–7]. However, the choice of interlayer, its thickness and dielectric permittivity has also a great importance to specify the performance and reliability of these structures [2, 3, 8–10]. Such an interlayer provides continuously control on the formation of barrier height (BH) at MS interface and conduction mechanisms [10–15]. In order to develop higher performance and cost-effective electronic devices compared to traditional oxide interlayer, new materials made using flexible, easily processable interlayers with metal or graphene additive have become more important [11, 12, 16–20]. Usually, the semi-logarithmic forward biases *I–V* curve in metal/insulator/semiconductor (MIS) and metal/polymer/semiconductor (MPS) type SBDs at moderate voltages ($V\leq3kT/q$) has a distinct linear behavior, but it may be deviation from the linearity at high voltages or currents due to the existence of R_s and interlayer [16–21]. The formation of R_s are usually depends on contacts (rectifier and ohmic), the existence of native or deposited interlayer at junction, resistivity of bulk semiconductor, non-uniform doping atoms and some impurities or dislocations in the semiconductor [1, 5, 9, 18–21]. These impurities or N_{ss} may be source from the interruption of the periodic lattice structure of semiconductor crystal, trapped charges and mobile ionic charges which can exchange with semiconductor in a short time [1, 4]. In the ideal case, the value of capacitance is independent from frequency, but in the applications especially at low frequencies this situation may be considerably different because the effect of N_{ss}, polarization and interlayer. For example, in recently, an anomalous peak was found in the forward bias C–V curves [22–27] due to the existence of N_{ss}, R_s and interlayer. The origin of the excess capacitance was attributed to the minority-carrier injection by Werner et al. [27].

It is well known that an interfacial insulator layer with low-dielectric constant such as SiO_2 and SnO_2 formed on a

✉ Selçuk Demirezen
selcukdemirezen@gmail.com

[1] Sabuncuoğlu Şerefeddin Vocational School of Health Services, Amasya University, Amasya, Turkey

semiconductor by the conventional methods such as thermal oxidation cannot completely passivate the active dangling bonds at the semiconductor surface and at M/S interface. Therefore, in the last two decades, many researchers purpose improving the electrical, optic, and dielectric characteristics of MS structures/contacts especially by using an interfacial polymer layer because of their high surface area to volume rate, light weight, good mechanical strength, charge storage capacity, flexibility, high dielectric strength, and easy processing techniques including an electrospinning, solid–liquid phase separation and template synthesis [16–18]. Additionally, among many polymers in the recently, especially polyvinyl alcohol (PVA) has become a great interest as a research topic due to its higher water solubility, process ability, higher film formation capacity and can be increased/improved its conductivity. The increase conductivity in these polymers are the result of high physical interactions between organic polymer chains, via hydrogen bonding between the hydroxyl groups and the dopant materials. In order to increase the value of capacitance ($C=\varepsilon'\varepsilon oA/di$) of these structures, one has to increase of dielectric constant (ε') or the electrode area (A) and the decrease of interfacial layer (d_i), but the value of d_i is largely determined by the working voltage and cannot be tempered. In addition, such high value of dielectric interlayer does not only prevent inter-diffusion between metal and semiconductor, it also alleviates the electric field reduction issue in these structures [2, 6, 10, 21, 25].

Additionally, the electrical characteristics of MS structure with and without a native or deposited interlayer may very different even if they identically prepared/fabricated. Therefore, in this study, the (Ni-doped PVA) polymer was used an interfacial layer at Al/p-Si (M/S) interface to be either or not a good candidate/suitable for BH modification at interface. The dielectric value of used (Ni-doped PVA) interlayer was found as 1.44 from the interlayer capacitance ($C_i=\varepsilon'\varepsilon_o A/d_i$), by taken the interlayer thickness as 10 nm, even at 20 kHz. This value is higher than the dielectric value of SiO_2 at 20 kHz. In addition, the value of dielectric can be increased by increasing a dopant level of Ni until at about 5–7%. Due to these reasons, in recent years, the MS structures with a polymer interlayer becomes more important research tools in the characterization of new semiconductor materials for the applications in the device technology in recent years.

In this work, we prepared composites of PVA and inorganic salt nickel acetate [$Ni(CH_3COO)_2 2H_2O$] in order to improve the bulk mechanical and electrical properties. The first aim of this work is to investigate the effects of the N_{ss}, R_s, and organic interlayer on the forward bias I–V and reverse bias C–V–f characteristics. The second aim is to determine the sources of difference between main electrical parameters depend on used calculated methods which are corresponding various applied bias voltage. For these purposes, C–V–f measurements were performed between 20 kHz and 1 MHz in wide range of bias voltages. Both the N_{ss} versus (E_{ss}–Ev) and ln(I)–ln(V) plots were also obtained from the forward bias I–V data to obtain more information on the possible conduction mechanisms depend on voltage.

2 Experimental details

The Al/(Ni-doped PVA)/p-Si (MPS) type SBDs have been fabricated on boron-doped (p-Si) wafer with (100) orientation, 2 inch (= 5.08 cm) diameter, 5 Ω.cm resistivity and 350 μm thickness. Si wafer was cleaned with RCA cleaning procedure and then dried with dry N_2 gas and then was dipped in ammonium peroxide for 40 s. to remove native oxide layer on the surface of Si and subsequently etched in the (H_2SO_4:H_2O_2:H_2O = 3:1:1) acid solutions for 10 min. After that it was rinsed in high-pure deionized water with 18 MΩ resistivity at 10 min. At last step, it was dried with N_2 gas and then immediately it was transferred in the high-vacuum thermal evaporation system and so high-pure Al with 120 nm thickness was evaporated onto the back side of it at 10^{-6} Torr. In order to get low-resistivity ohmic contact, Al/p-Si was annealed at 500 °C in N_2 ambient at 5 min. In this study, (Ni-doped PVA) organic material was used an interfacial layer due to its high surface area to volume rate, light weight, good mechanical strength, charge storage capacity, flexibility, high dielectric strength, and easy processing techniques such as electrospinning, solid–liquid phase separation and template synthesis. Additionally, PVA has become a great interest as a research topic due to its higher water solubility, process ability, higher film formation capacity and can be increased/improved its conductivity. The prepared (Ni-PVA) solution was grown by electrospinning method as given Fig. 1. "Electro spinning process" utilizes electrical force to produce polymer fibers and it has four major components: The high voltage–power supply (HVPS), the spinneret, the syringe pump and the electrically conductive collector. In this system, using a peristaltic syringe pump, the precursor solution was delivered to a metal needle syringe (10 ml), with an inner diameter of 0.9 mm, at a constant flow rate of 0.05 ml/h for obtaining nanofibers onto substrates. The needle was connected to a HVPS and positioned vertically on a clamp. A piece of flat aluminum foil was placed 18 cm below the tip of the needle to collect the nanofibers and then p-Si wafer was placed on the aluminum foil. Upon applying a high voltage of 17 kV on the needle, a fluid jet was ejected from the tip. The prepared-composite film (0.01 Ni-doped PVA) was deposited onto the top-polished surface of p-Si wafer using the electro-spinning technique. Finally, the circular dots of 1 mm in diameter ($=7.85\times10^{-3}$ cm^2 area) and 120 nm thickness of high-pure Al rectifier contacts were evaporated on the front of p-Si surface at 10^{-6} Torr.

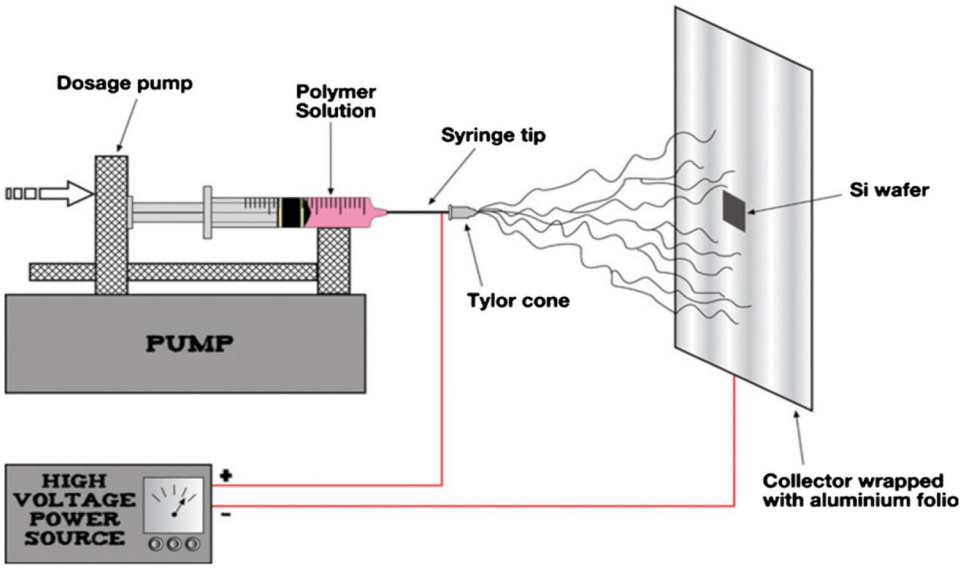

Fig. 1 The simple illustration of the electrospinning system

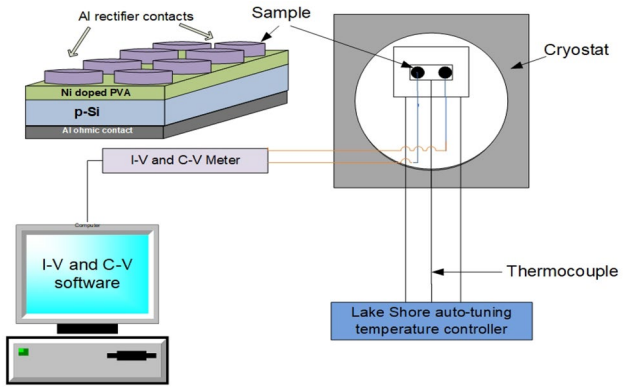

Fig. 2 Schematic model of the (Al/(Ni-PVA)/p-Si MIS) structures and measurement system

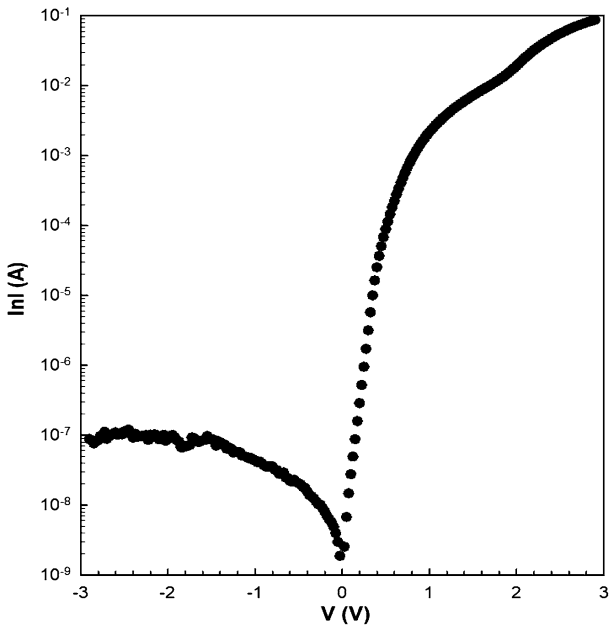

Fig. 3 The semi-logarithmic forward and reverse bias I–V plots for the MPS type SBD

In order to perform both the I–V and C–V–*f* measurements, the prepared samples were mounted on a Cu-holder with a Ag-paste and then electrical connections were made to the upper rectifier contact using Ag-coated Cu wires with Ag-paste. I–V and C–V–*f* measurements were controlled by a microcomputer through an IEEE-488 ac/dc converter card by utilizing a source meter (Keithley 2400) and an impedance analyzer (HP 4192 A LF), respectively. Both the schematic model of the fabricated (Al/(Ni-PVA)/p-Si) (MIS)-structures and measurements system were given in Fig. 2, respectively.

3 Results and discussions

3.1 The current–voltage (I–V) characteristics

Figure 3 shows the forward and reverse bias lnI–V plot of the MPS type SBD. As shown in Fig. 3, the semi-logarithmic ln*I*–*V* plot in the forward bias region has a good linear regime at intermediate bias voltages. But, the ln*I*–*V* plot is also considerably deviated from the linearity at sufficiently high forward bias voltages ($V \geq 0.5$ V) due to the existence a high series resistance (Rs) of structure and (Ni-doped PVA) organic interlayer between Al and p-Si [24–30]. In this case, the applied bias voltage on the diode will be shared between Rs, interlayer and depletion layer of the diode depend on their magnitudes. In other words, the forward bias current keeps increasing with increasing

forward bias voltage however deviation from the linearity occurs because of increasing voltage drop due to Rs and interlayer (Va = IRs + Vi + Vd) towards for enough higher biases. On the other hand, the observed non-saturation behavior at reverse biases is the result of the image-force lowering barrier height (BH), generation-recombination (GR), and the existence of interlayer. Such non-saturating reverse bias I–V characteristics is believed to stem from the contribution of recombination current and the contribution due to lowered BH induced by image-force and the existence of many patches or pinch-off at M/S interface [31, 32]. It is clear that the rectifying rate (RR = IF/IR) at ± 3 V is considerably high when compared a conventional Al/p-Si (MS) type Schottky barrier diodes (SBDs) [15, 16]. These results show that (Ni-PVA) interlayer supplied better performance in respect of low-value of leakage current and high-value of RR so that can be successfully used an alternative interlayer for replacing traditional oxide or insulator interlayer.

For a SBD with an interlayer and Rs, the relation between I and V on the base of thermionic emission (TE) (V > 3kT/q) is given as following [1–5]:

$$\begin{aligned} \mathrm{I} &= AA^{*}T^{2}\exp(-\frac{q}{kT}\Phi_{Bo})\left[\exp\left(\frac{q(V-IR_{s})}{nkT}\right)-1\right] \\ &= \mathrm{I}_{0}\left[\exp\left(\frac{qV_{D}}{nkT}\right)-1\right] \end{aligned} \quad (1)$$

In Eq. 1(a), the quantities of I_o, V, n, IR_s are the reverse-saturation current, applied voltage across the SBD, voltage drops on the R_s, ideality factor, respectively. Both the value of I_o and n can be calculated from the intercept and slope of the linear regime of ln(I)–V plot by using ln(I) = Ln(I_o) + (q/nkT)V relation. The value of n is a measure of conformity of the diode to pure TE theory. Thus, the value of zero-bias BH (Φ_{Bo}) can be calculated from Eq. 1 using the experimental value of I_o and the rectifier contact area (A) as following:

$$\Phi_{Bo} = \frac{kT}{q}Ln\left(\frac{AA^{*}T^{2}}{I_{0}}\right) \quad (2)$$

The I_o, n, and Φ_{Bo} values for the MPS type SBD were found as 2.14×10^{-9} A, 1.606 and 0.750 eV, respectively. The rectifying rate ($RR = I_F/I_R$) at ± 3 V was calculated as 10^6. It is clear that the high value of n is higher than unity due to the existence of interlayer, a particular distribution of N_{ss}, inhomogeneity of BH at Al/p-Si interface, and interface recombination [5–9]. In order to determine the dominant current-transport mechanism, ln(I)−ln(V) plot was also drawn and is given in Fig. 4.

It is clear that the ln(I)−ln(V) plot has four linear regimes and usually exhibits a power-law behavior ($I \propto V^m$). For R1 (low bias voltages), the value slope (m) is lower than 2 indicating the current-transport (CT) almost governed by the Ohm's Law. For RII (moderate bias voltages) m is considerably greater than 2 indicating CT is governed by the trap-charge-limited current (TCLC) according to this mechanism, the increase in the number of injected electrons causes filling of traps and so filled traps lead to the increase of the space charges [33–35]. For RIII and IV (at higher voltages), the values of m tend to decrease again as the sample approach the "trap-filled" limit due to the strong electron injection. In this case, electrons (escaped from the traps) contributed to the space-charge- limited current (SCLC) [21–23].

The existence of Rs in MIS and MPS type SBDs can be considerably affected the I-V and C-V characteristics at enough high forward bias voltages and it is usually calculated from the Ohm's Law, Norde function [36], Cheung's functions [37], Nicollian-Brews method [9]. Firstly, the value of resistance (R_i)–V plot was obtained from Ohm's Law ($Ri = dV_i/dI_i$) is given in Fig. 5. As shown in Fig. 5, the value of R_i reach a constant for higher forward voltages which is corresponding to the real value of R_s, but its constant value at enough high reverse voltages is corresponding to the real value of shunt-resistance (R_{sh}). These values were found as 31.5 Ω and 37.5 MΩ at ± 3 V, respectively.

Since the lnI–V plot at the forward bias voltage region has not distinct with each other or has narrow linear region, the reliability and accuracy of calculated electrical parameters in this region become decreases. In this case, a new method introduced by Norde was used for n = 1 and then it was modified for very higher values of n [36, 38]. In this way, the main electrical parameters can be calculated from the forward bias I-V data using Eq. 3.

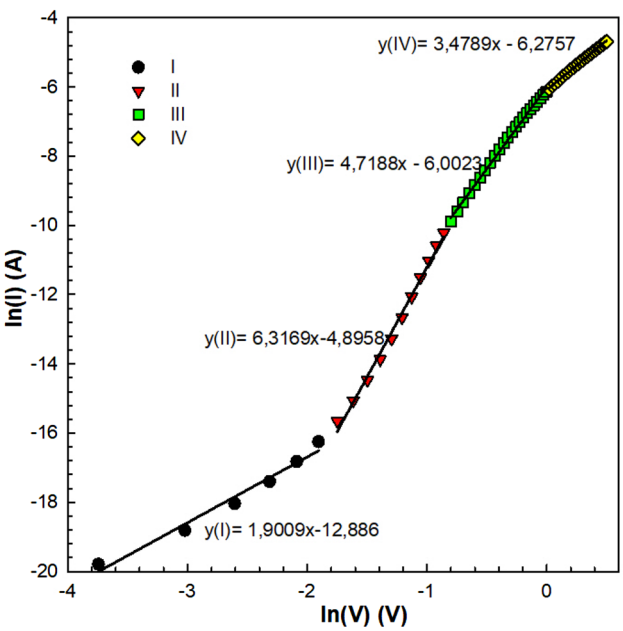

Fig. 4 The forward bias ln(I)–ln(V) plot for the MPS type SBD

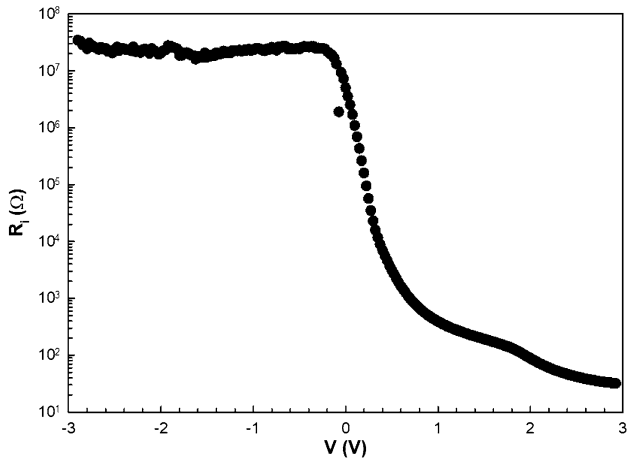

Fig. 5 $\ln R_i$–V plot for the MPS type SBD obtained from Ohm's law

$$F(V) = \frac{V}{\gamma} - \frac{\mathrm{kT}}{q}\left(\frac{I(V)}{AT^2}\right) \tag{3}$$

In Eq. 3, γ is a constant and it must be greater than n. The F(V)–V plot was drawn using Eq. 3 and is given in Fig. 6. As shown in Fig. 6, F(V)–V plot has a minimum point corresponds to the $F(V_{min})$ and V_{min}. Thus, the value of R_s and BH for SBD can be calculated from Eqs. 4 and 5 as a second way, respectively [38]:

$$R_s = \frac{kT(\gamma - \mathrm{n})}{qI_{\min}} \tag{4}$$

$$\Phi_B = F(V_{\min}) + \frac{V_{\min}}{\gamma} - \frac{kT}{q} \tag{5}$$

Thus, the values of R_s and Φ_B were calculated from Eqs. (4) and (5) as 95,74 Ω and 0.703 eV, respectively.

The third way to determine n, Φ_B and R_s values are uses the Cheungs' functions from the concave curvature of the lnI–V plot by using Eqs. 6 and 7, respectively [25]:

$$\frac{dV}{d(\ln I)} = n\left(\frac{kT}{q}\right) + R_s I \tag{6}$$

$$H(I) = V - \mathrm{n}\left(\frac{\mathrm{kT}}{q}\right)\ln\left(\frac{I}{\mathrm{AA}^{*}T^2}\right) = \mathrm{n}\Phi_B + R_s I \tag{7}$$

Figure 7 shows the experimental dV/dln(I)–I and H(I)–I plots of the MPS type SBD and have a good linear region. Firstly, the values of n and R_s were obtained from the intercept and slope of the dV/dln(I)–I plot by fitting Eq. 6 as 6.32 and 11.56 Ω, respectively. Secondly, by using this value of n, the values of R_s and Φ_B were obtained from the slope and intercept of H(I)–I plot by fitting Eq. 7 as 9.16 Ω, 0.637 eV, respectively. The discrepancy between TE and Cheung

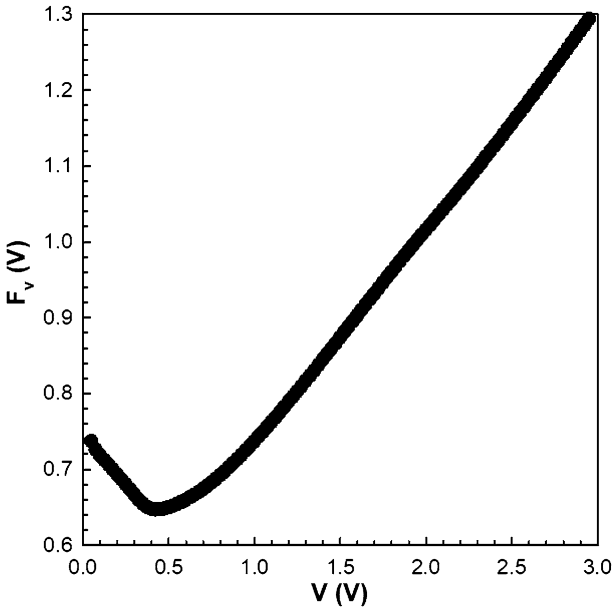

Fig. 6 The F(V)–V plot for the MPS type SBD

functions of these values is the result of voltage dependent of them and a special distribution of N_{ss} at interlayer/p-Si interface located at band gap of semiconductor.

The existence of N_{ss} are usually raised from the semiconductor surface imperfection like doping bonds, oxygen vacancies, structural rearrangements due to metallization, doping atoms and interlayer which are also more effective on the I–V and C–V characteristics of these structures. According to Card and Rhoderick [28], the value of n becomes greater than unity due to the existence interlayer thickness

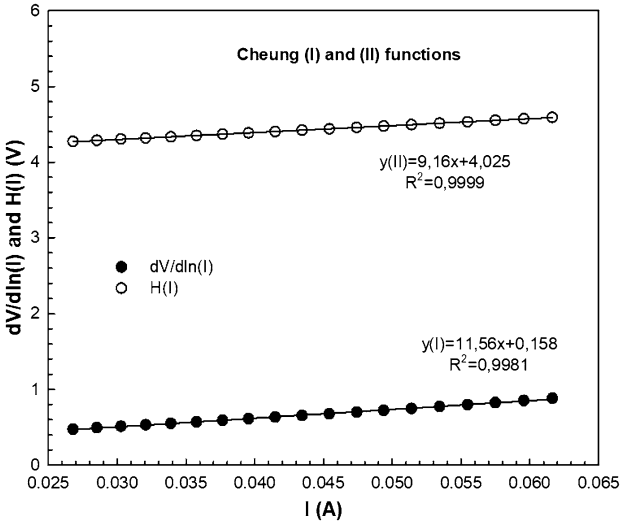

Fig. 7 The dV/dlnI–I and H(I)–I plots the MPS type SBD

(δ), N_{ss}, and thicknes of depletion layer (W_D) as seen in Eq. 8:

$$n(V) = \frac{q}{kT}\left[\frac{(V - IR_s)}{\ln(I/I_o)}\right] = 1 + \frac{\delta}{\varepsilon_i}\left[\frac{\varepsilon_s}{W_D} + qN_{ss}(V)\right] \quad (8)$$

Here, ε_s and ε_i are the dielectric of semiconductor and interlayer, respectively. The values of W_D and δ were calculated from the C–V plot as following Sect. 3.2. The voltage dependent BH is given Eq. 9 [1, 4, 28].

$$\Phi_e = \Phi_{BO} + \beta(V - IR_s) = \Phi_{BO} + \left(1 - \frac{1}{n(V)}\right)(V - IR_s) \quad (9)$$

where β (=dΦe/dV = 1 − 1/n(V)) is the voltage coefficient of BH used in the place of the Φ_{Bo}. Thus, the energy dependent profile of N_{ss} can be extracted from Eqs. 10 and 11 as the follows [1, 18, 28]:

$$N_{ss}(V) = \frac{1}{q}\left[\frac{\varepsilon_i}{d}(n(V) - 1) - \frac{\varepsilon_s}{W_D}\right] \quad (10)$$

For p-type semiconductors, the energy level of N_{ss} with respect to the bottom of E_v is given Eq. 11 [1, 18].

$$Ec - Ess = q(\Phi_e - V) \quad (11)$$

Thus, the N_{ss} vs (E_{ss}–E_v) for the MPS type SBD was obtained using Eqs. 10, 11 and is given in Fig. 8. As shown in Fig. 8, there is an exponential growth of the N_{ss} from mid-gap of Si towards the bottom of E_v and their mean value has 10^{12} eV^{-1} cm^{-2} order which are suitable for the MPS type SBD.

3.2 The capacitance–voltage–frequency (C–V–f) characteristics

The impedance or admittance (Z = 1/Y) measurement is based on measuring the capacitance (Cm) and conductance (Gm/ω) of a MS type structure with an interfacial insulator or polymer layer (MIS or MPS) as a function of bias voltage and frequency. The frequency dependence is related to the characteristic trap response time (τ = 2π/ω), where ω is the angular frequency. In generally, the obtained value of BH from the reverse bias C–V data is higher than the forward bias I–V data as almost E_F level because of the apparent BH from metal to semiconductor is lower than from semiconductor to metal. In addition, the measured C–V data are considerably dependent of frequency, N_{ss} and their life time (τ) and usually decrease with increasing frequency because of the charges at traps can follow to the external ac signal [1, 3, 9, 28]. But, sometimes, the C–V plots give an anomalous peak in depletion and accumulation region due to the existence of N_{ss} and R_s, respectively. As shown Fig. 9, the value of C decrease with increasing frequency and C–V plot has a peak for each frequency at

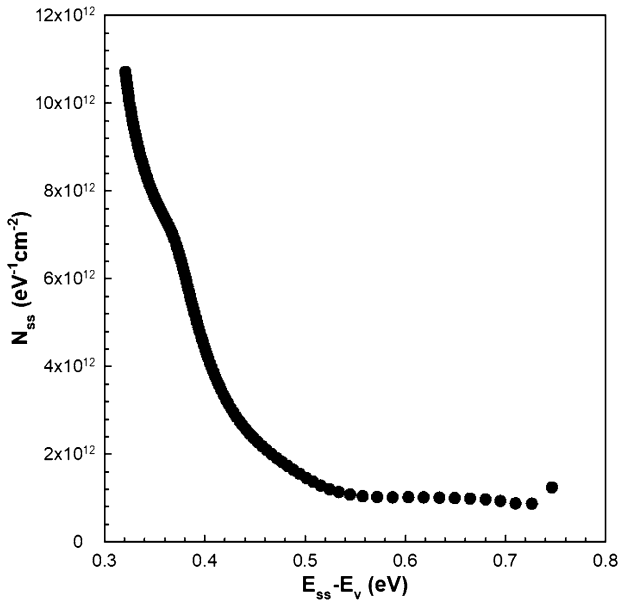

Fig. 8 The N_{ss}–(E_{ss}–E_v) plot for the MPS type SBD

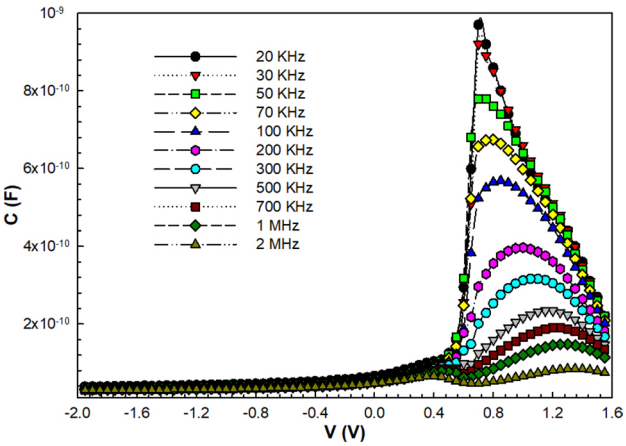

Fig. 9 The forward and reverse bias C–V plots of the MPS type SBD for various frequencies

accumulation region due to the effect of R_s rather than organic interlayer because of the magnitude of N_{ss} decrease with increasing frequency and shift towards accumulation region due to a special distribution of N_{ss} under electric field.

The relation between measured C and V for MIS and MPS type SBDs can be expressed as [1–4].

$$\frac{1}{C^2} = \frac{2}{q\varepsilon_s\varepsilon_0 N_A A^2}\left(V_{bi} - \frac{kT}{q} - V_R\right) \quad (12)$$

Here, V_R is the reverse bias voltage and V_{bi} is the built-in voltage. The values of V_{bi} and N_A can be obtained from the extrapolation of the C^{-2}–V plot to the x-axis (V) and slope

of this plot for each frequency. Therefore, the C^{-2}–V plots were drawn between 20 kHz and 1 MHz and are presented in Fig. 10, respectively.

As can be seen from the C^{-2}–V plots (Fig. 10) have a good linear regime when these measurements are performed at intermediate and high frequencies indicated that the value τ closer to the period or lower (T = 1/2πf) [4, 9, 28]. Thus the value diffusion potential ($V_d = V_o + kT/q$), E_F, and the doping atoms (N_A) are calculated from the intercept and slope ($\tan(\theta) = dC^{-2}/dV$) of the C^{-2}–V plot for each frequency by using Eqs. 13, 14, 15, respectively, and are tabulated in Table 1 [8, 28, 30]:

$$N_A = 2/\left(q\varepsilon_s\varepsilon_o A^2 tan(\theta)\right) \tag{13}$$

$$E_F = kT/qln(N_V/N_A) \tag{14}$$

In Eq. 14, N_V is the effective density of states in Si valance band. Thus, the value of the BH ($\Phi_{B(C-V)}$) can be calculated Eq. 15 as following [4, 9]:

$$\Phi_B(C-V) = \left(V_0 + \frac{kT}{q}\right) + \frac{kt}{q\ln\left(N_V/N_A\right)} = V_D + E_F \tag{15}$$

As shown in Table 1, the V_D, N_A, E_F, W_d and $\Phi_{B(C-V)}$ values of the MPS type SBD are function of frequency due to N_{ss} and organic interlayer polarization under electric field. As can be clearly seen in Table 1, the values of N_a decrease with increasing frequency, conversely $\Phi_{B(C-V)}$, W_D, and E_F increases. In addition, there is almost a linear relationship between $\Phi_{B(C-V)}$ and frequency. The obtained experimental results show that N_{ss} and polarization are effective in the weak inversion and depletion regions for low and intermediate frequencies, R_s and interlayer are effective only at accumulation region. The observedw some discrepancy between in the electrical parameters was attributed to the voltage-dependent of them and the nature of the calculation method. It is clear that the value of $\Phi_{B(C-V)}$ for each frequency is higher than obtained from forward bias I–V plot by using TE and Cheungs' functions. This discrepancy can be attributed to the nature of measurement method. As a result, all experimental results show that the values of N_{ss}, R_s, and organic interlayer are more effective both in the I–V and C–V–*f* characteristics and so they must be taken into account in the investigation of electrical characteristics.

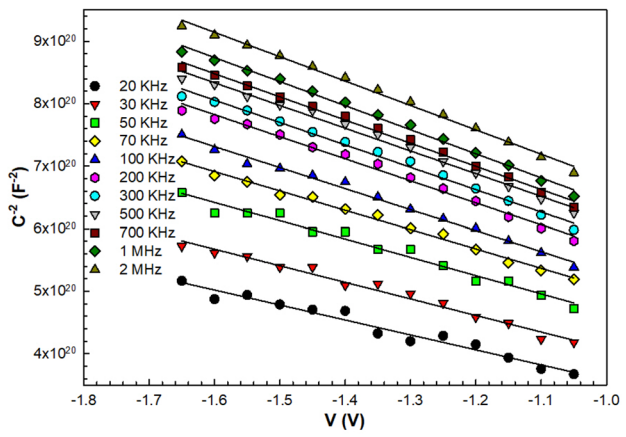

Fig. 10 The reverse bias C^{-2}–V plots of the MPS type SBD for various frequencies

Table 1 Some experimental values of V_o, N_a, E_F, $\Phi_{B(C-V)}$, and W_d obtained from the reverse bias C^{-2} versus V plots for the MPS type SBD for various frequencies

f (kHz)	V_o (eV)	$N_a \times 10^{14}$ (cm^{-3})	E_F (eV)	Φ_B(c-v) (eV)	$W_d \times 10^{-5}$ (cm)
20	0.496	6.20×10^{14}	0.244	0.765	8.94×10^{-5}
30	0.511	6.94×10^{14}	0.248	0.784	9.80×10^{-5}
50	0.532	5.94×10^{14}	0.252	0.809	1.08×10^{-4}
70	0.560	5.55×10^{14}	0.253	0.838	1.15×10^{-4}
100	0.577	5.78×10^{14}	0.252	0.855	1.14×10^{-4}
200	0.618	5.50×10^{14}	0.254	0.896	1.21×10^{-4}
300	0.651	5.43×10^{14}	0.254	0.930	1.25×10^{-4}
500	0.674	5.19×10^{14}	0.255	0.954	1.30×10^{-4}
700	0.687	5.24×10^{14}	0.255	0.967	1.31×10^{-4}
1000	0.707	5.32×10^{14}	0.254	0.986	1.32×10^{-4}
2000	0.744	4.98×10^{14}	0,256	1.025	1.40×10^{-4}

4 Conclusions

In order to determine the effects of R_s, N_{ss} and (Ni-PVA) organic interlayer on the electrical characteristics both the forward and reverse bias I–V and C–V–f measurements were performed at room temperature. Firstly, the main electrical parameters of the MPS type SBD such I_o, n, Φ_{Bo}, RR, R_s, and R_{sh} were found as 2.14×10^{-9} A, 1.606, 0.750 eV, 1.07×10^6, 30.4 Ω and 37.7 MΩ from the I–V characteristics, respectively. The energy dependent (E_{ss}–E_v) profile of the N_{ss} was also extracted from the forward bias I–V data by using voltage dependent of BH and n with 10^{12} eV^{-1} cm^{-2} order which is more suitable when compared conventional of MIS type SBDs. In order to determine the possible CT mechanisms, he forward bias ln(I)–ln(V) plot was drawn ant it shows four linear sections with different slopes (m) and usually shows a power-law behavior ($I \propto V^m$). On the other hand, the other N_a, E_F, Φ_B(C–V, and W_D values obtained from the reverse bias C^{-2}–V between 20 and 20000 kHz and they were changed from the 6.20×10^{14} cm^{-3}, 0.244 eV, 0.765 eV, 8.94×10^{-5} cm (at 20 kHz) to 4.98×10^{14} cm^{-3}, 0.256 eV, 1.025 eV, 14.0×10^{-5} cm at 2 MHz from the linear part of reverse bias C^{-2}–V plots respectively. All these

results show that the N_{ss}, R_s and (Ni-doped PVA) organic inter-layer have significant effects both on the I–V and C–V–f characteristics of the SBDs. As a result, all experimental results show that the values of N_{ss}, R_s, and organic interlayer are more effective both in the I–V and C–V–f characteristics and so they must be considered in the investigation of electrical characteristics.

Acknowledgements This work is supported by Amasya University BAP research Project with FMB-BAP 17-0292 number. The author wishes to express his gratitude to Prof. Dr. Şemsettin Altındal for his abundantly helpful support and guidance.

References

1. B.L. Sharma, *Metal-semiconductor Schottky Barrier Junctions and Their Applications* (Plenum Press, New York, 1984)
2. H. Tecimer, A. Türüt, H. Uslu, Ş. Altındal, İ. Uslu, Sens. Actuators A **199**, 194 (2013)
3. J. Werner, H. Guttler, J. Appl. Phys. **69**, 1522–1533 (1991)
4. S.M. Sze, *Physics of Semiconductor Devices* (Wiley, New York, 1981)
5. E. Özavcı, S. Demirezen, U. Aydemir, S. Altındal, Sens. Actuators A **194**, 259 (2013)
6. Ş. Altındal, J. Mater. Electron Dev. **1**, 42 (2015)
7. R.T. Tung, J.P. Sullivan, F. Schrey, Mater. Sci. Eng. B **14**, 266 (1992)
8. W. Mönch, J. Vac. Sci. Technol. B **17**, 1867 (1997)
9. E.H. Nicollian, J.R. Brews, *Mos (Metal Oxide Semiconductor) Physics and Technology* (Wiley, New York, 1982)
10. S. Demirezen, A. Kaya, Ö. Vural, Altindal. Mater. Sci. Semicond. Process. **33**, 140–148 (2015)
11. S. Altındal Yerişkin, M. Balbaşı, İ. Orak, J. Mater. Sci. **28**, 14040–14048 (2017)
12. M. Sharma, S.K. Tripathi, Appl. Phys. A **113**, 491–499 (2013)
13. C. Tozlu, A. Mutlu, Synth. Met. **211**, 99–106 (2016)
14. V.R. Reddy, Thin Solid Films **556**, 300–306 (2014)
15. M.S.P. Reddy, H.-S. Kang, J.-H. Lee, V.R. Reddy, J.-S. Jang, J. Appl. Polym. Sci. **131**, 131 (2014). https://doi.org/10.1002/app.39773
16. S. Boughdachi, Y. Badali, Y. Azizian-Kalandaragh, Ş. Altindal, J. Electron. Mater. **47**, 6945–6953 (2018)
17. E.A. Akhlaghi, Y. Badali, Ş. Altindal, Y. Azizian-Kalandaragh, Phys. B **546**, 93–98 (2018)
18. Y. Badali, A. Nikravan, Ş. Altindal, İ. Uslu, J. Electron. Mater. **47**, 3510–3520 (2018)
19. Serhat Orkun Tan, J. Polytech. **21**(4), 977–989 (2018)
20. S.O. Tan, IEEE Trans. Electron Devices **64**, 5121–5127 (2017)
21. S. Alialy, Ş. Altındal, E.E. Tanrıkulu, D.E. Yıldız, J. Appl. Phys. **116**, 083709 (2014)
22. P.S. Ho, E.S. Yang, H.L. Evans, X. Wu, Phys. Rev. Lett. **60**, 177 (1986)
23. X. Wu, E.S. Yang, J. Appl. Phys. **65**, 3560 (1989)
24. P. Chattopadhyay, B. Raychaudhuri, Solid State Electron. **35**, 875 (1992)
25. Ç. Bilkan, A. Gümüş, Ş. Altındal, Mat Sci Semicond Process **39**, 484 (2015)
26. B. Bati, C. Nuhoğlu, M. Sağlam, E. Ayyildiz, A. Türüt, Phys. Scrıpta **61**, 209 (2000)
27. J. Werner, A.F.J. Levi, R.T. Tung, M. Anzlowar, M. Pinto, Phys. Rev. Lett. **60**, 53 (1988)
28. H.C. Card, E.H. Rhoderick, J. Phys. D **4**, 1589 (1971)
29. S. Alialy, A. Kaya, E. Marıl, S. Altındal, I. Uslu, Phil. Mag. **95**, 1448 (2015)
30. S. Altındal Yerişkin, J Mater Sci: Mater Electron **30**, 17032 (2019)
31. İ. Taşçıoğlu, S.O. Tan, F. Yakuphanoğlu, Ş. Altındal, J. Electron. Mater. **47**, 6059–6066 (2018)
32. S. Altındal Yerişkin, M. Balbaşı, S. Demirezen, Indian J. Phys. **91**, 421–430 (2017)
33. V. Rajagopal Reddy, V. Manjunath, V. Janardhanah, Y.-H. Kıl, C.-J. Choı, J. Electron. Mater. (2014). https://doi.org/10.1007/s11664-014-3177-3
34. Y.S. Ocak, M. Kulakcı, T. Kılıcoğlu, R. Turan, K. Akkılıc, Synth. Met. **159**, 1603 (2009)
35. V.R. Reddy, V. Janardhanah, J.-W. Ju, H.-J. Yun, C.-J. Choi, Solid State Commun. **179**, 34 (2014)
36. H. Norde, J. Appl. Phys. **50**, 5052 (1979)
37. S.K. Cheung, N.W. Cheung, Appl. Phys. Lett. **49**, 85 (1986)
38. A.A.M. Farag, A. Ashery, E.M.A. Ahmed, M.A. Salem, J. Alloys Compd. **495**, 116 (2010)